RSC Advances

PAPER

View Article Online
View Journal | View Issue

Check for updates

Cite this: *RSC Adv.*, 2017, **7**, 20116

Ferrimagnetic half-metallic properties of Cr/Fe δ doped MoS_2 monolayer

M. D. Xie,[a] C. G. Tan,*[a] Pan Zhou,[a] J. G. Lin[b] and L. Z. Sun*[b]

Received 4th January 2017
Accepted 18th March 2017

DOI: 10.1039/c7ra00133a

rsc.li/rsc-advances

Using first-principles calculations, we found that Cr/Fe δ-type doping is an effective approach to modulate the electronic and magnetic properties of monolayer MoS_2. Distinguished from ferromagnetic half-metallic Fe δ-type doped MoS_2, Cr and Fe alternately δ-type codoped MoS_2 presents half-metallic ferrimagnetism. The 3d orbitals of Cr and Fe strongly couple with the p states of their nearest neighbor S, and virtual hopping between them follows the GKA rules, thus the antiferromagnetic superexchange interaction between Cr and Fe produces the ferrimagnetic nature of the system. Our results indicated that the 3d δ-type doping in monolayer MoS_2 provides an effective approach to produce a one dimensional spin-polarized transport channel.

Open Access Article. Published on 06 April 2017. Downloaded on 1/20/2026 4:31:29 AM.
This article is licensed under a Creative Commons Attribution-NonCommercial 3.0 Unported Licence.

1 Introduction

Since de Groot[1] proposed the concept of half-metallic ferromagnets (HMFs) from the band structure of NiMnSb, HMFs have been a hot research topic during the last few decades due to their potential applications in spintronics. Half-metal materials, with 100% spin-polarized[2] conduction electrons at the Fermi level, are a class of special magnetic materials that can be used as magnetic layers in magnetic tunnel junctions to obtain prodigious magnetoresistance.[3] Lately, lots of materials have been predicted theoretically to exhibit this particular behavior, such as rutile CrO_2[4] and mixed-valence perovskite Mn-doped GaAs.[5]

Although the HMF shows great potential in spintronics, the magnetic domains and stray field in the system due to its ferromagnetic (FM) nature will inevitably restrict the generation of a spin-polarized current. van Leuken and de Groot[6] proposed that this half-metallic nature can be achieved in antiferromagnets (HMAs) or ferrimagnets (HMFi's), which will overcome the drawbacks of HMFs due to their zero or smaller magnetization. HMAs, with half-metallic characteristics but without any net magnetization, have been theoretically predicted in $V_7MnFe_8Sb_7In$ alloys,[6] perovskite oxides,[7,8] Mott insulator NiO,[9] monolayer superlattices,[10] and diluted magnetic semiconductors.[11] All of them show potential applications in novel spin-polarized STM tips,[6] new spin injection devices, and single spin superconductivity.[7] Besides HMAs, HMFi's also aroused a lot of concerns due to their lower total magnetic moments in comparison to those of HMFs. van Leuken and de Groot[6] theoretically proposed that FeMnSb is half-metallic with a net moment of only 2 μ_B due to the antiparallel spin moments between Fe and Mn behaving as HMFi's. HMFi's create smaller external magnetic fields and this results in smaller energy losses in comparison to HMFs. In addition, HMFi's provide the prototypic template for designing HMAs. For example, starting from Mn_2VAl and Mn_2VSi Heusler alloys which are well known HMFi's, Galanakis *et al.*[12] obtained a desirable HMA by substituting Co and Fe for Mn.

Traditionally, HMAs and HMFi's were realized in complex crystal structures such as perovskite cuprates. The complex structures may suppress their magnetic properties owing to the lattice distortions in the systems.[3] In comparison with the materials mentioned above, two dimensional (2D) materials, especially the 2D materials with large band gaps, are more suitable for spintronics due to their simple structures and easily controllable magnetic properties.[13] In our previous work,[14,15] half-semiconductor antiferromagnets with vanishing net magnetization were proposed in 2D h-BN, GaN, AlN, and Janus MXenes, paving the way for HMAs in 2D materials. One of the most recently obtained 2D materials, MoS_2, with an S–Mo–S sandwich structure, is a direct band gap semiconductor with a band gap of 1.8 eV,[16] which is potentially useful in transistors,[17] phototransistors,[18] gas transducers,[19] lithium and sodium batteries, and solar cells.[20–22] Experimentally, mono- and multi-layer MoS_2 have been successfully fabricated through various methods including chemical vapor deposition,[23] a liquid exfoliation method,[24] mechanical exfoliation,[25] and sulfurization of a pre-deposited transition metal or transition metal oxide.[26,27] The pristine MoS_2 analogous to graphene is a nonmagnetic material. To promote its applications in spintronics, methods including cutting the material into zigzag MoS_2 nanoribbons,[28] transitional metal (TM) adsorption,[29,30]

[a]*Key Laboratory of Low-Dimensional Materials and Application Technology, School of Material Sciences and Engineering, Xiangtan University, Xiangtan 411105, China. E-mail: gctan@xtu.edu.cn*

[b]*Hunan Provincial Key Laboratory of Thin Film Materials and Devices, School of Material Sciences and Engineering, Xiangtan University, Xiangtan 411105, China. E-mail: lzsun@xtu.edu.cn*

This journal is © The Royal Society of Chemistry 2017

Open Access Article. Published on 06 April 2017. Downloaded on 1/20/2026 4:31:29 AM.
This article is licensed under a Creative Commons Attribution-NonCommercial 3.0 Unported Licence.

and TM doping[31–34] were used. Among them, TM substitutional doping is one of the most simple and effective techniques to modulate the electronic and magnetic properties of MoS_2. Substitutional doping of various TM dopants at the S or Mo sites has been successfully used to modulate the magnetic and electronic structure of the MoS_2 monolayer.[31–34] In comparison with TM atom substitutional doping at the S site, the absolute value of the binding energy (E_b) indicates that TM doping at the Mo site is more stable.[35] However, substitutionally doping the TM atom at the Mo site only induces small magnetic moments, and the material still remains as a semiconductor with a narrower band gap.[36] Previous studies have indicated that a total magnetic moment of 2 μ_B is observed for Fe doping, but doping with Cr shows a Jahn–Teller distortion and consequently no magnetism.[36] Such results derive from single TM doping without considering the coupling between the TM dopants. The question is how the TM coupling influences the magnetic and electronic properties of the TM doped systems. Such an issue deserves more attention.

In this work, taking Cr/Fe, Cr, and Fe δ-type doped monolayer MoS_2 including four different configurations as examples, we investigate the influence of TM coupling on the magnetic and electronic properties of Cr/Fe δ doped monolayer MoS_2. We find that the Fe δ-type doped monolayer MoS_2 behaves as a HMF with a magnetic moment of 4 μ_B for each Fe. The results indicate that the coupling between Fe produces the high spin state of Fe in the system. As for the Cr δ-type doped system, the Cr anti-ferromagnets couple with each other, so the system behaves as a non-magnetic semiconductor. The Cr and Fe δ-type codoped material with a CrCrFeFe-chain-MoS_2 configuration is a metal. The neighboring CrCr, FeFe, and FeCr all show anti-ferromagnetic coupling, so these produced systems only show slight magnetic moments, while the system with an FeCrFeCr-chain-MoS_2 configuration behaves as a HMFi' with 100% spin-polarization even though the neighboring Fe and Cr show anti-ferromagnetic coupling. The system shows 2 μ_B magnetic moments per unit cell and the metallic characteristics derive from the spin-up channel contributed to by Fe and its neighboring S and Mo atoms. The anti-ferromagnetic coupling in the FeCrFeCr-chain-MoS_2 configuration follows the superexchange of the GKA rules. The results in the present work indicate that the δ-type doping in monolayer MoS_2 is an effective method to produce a one-dimensional spin-polarized transport channel.

2 Models and computational methods

Our calculations were performed using the spin-polarized density-functional theory (DFT),[37,38] as implemented in the Vienna *ab initio* simulation package (VASP).[39,40] The first-principles method adopted in our present work is suitable to study the electronic and magnetic properties of nano-magnetic materials, which has been proven by lots of previous reports.[41,42] Projector augmented wave (PAW)[43,44] potentials were used to describe the electron–ion interactions and the generalized gradient approximation (GGA) of Perdew, Burke, and Ernzerhof (PBE)[45] was adopted for electron exchange and correlation interactions. The plane-wave kinetic energy cutoff of 500 eV was employed, which is sufficiently large for our systems. For single Cr or Fe doped monolayer MoS_2, we adopted a 4×4 supercell containing 32 S, 1 Cr (or Fe) and 15 Mo. A gamma-centered $5 \times 5 \times 1$ *k*-mesh was applied for relaxation calculations and a $7 \times 7 \times 1$ *k*-sampling for static calculations. To investigate the δ-type doping of Cr and Fe in MoS_2, a large periodic supercell should be used in the calculation. We found that a 7×4 supercell is large enough by testing different supercell sizes. In the supercell, the Cr/Fe magnetic chain is along the *y*-axis, and the *x*-axis is greater than 19 Å to avoid interactions between the two Cr/Fe magnetic chains in the neighboring images. To avoid interaction between adjacent images, the vacuum region perpendicular to the sheet was set to 15 Å. The first Brillouin zone (BZ) was sampled by adopting $1 \times 5 \times 1$ and $3 \times 7 \times 1$ gamma-centered Monkhorst–Pack grids for geometry relaxation and electronic structure calculations, respectively. The criteria for the energy and atomic force convergence were set to 10^{-6} eV per unit cell and 0.01 eV $Å^{-1}$, respectively.

The electronic properties of the TM δ-type doped monolayer MoS_2 are sensitive to the treatment of the local Coulomb interactions U of the TM d orbital due to its strong localization. Therefore, DFT+U[46] is an essential approach to accurately investigate the electronic structures of Cr/Fe, Cr, and Fe δ-type doped monolayer MoS_2. In the present work, we perform GGA+U calculations and apply $U_{eff} = 4.0$ eV to the Cr and Fe atoms. We also test $U_{eff} = 3.0$ eV and $U_{eff} = 5.0$ eV, with the results revealing that there is no significant impact on the electric and magnetic properties upon changing the U_{eff} value. We tested the results of small size MoS_2 with 3d transition metal doping based on functional HSE06, which gave similar magnetic properties (the main point of our present work) with those based on PBE+U. Considering the time consuming nature of HSE06, we adopted PBE+U in the present work.

3 Results and discussions

We firstly studied the electronic and magnetic properties of single Cr/Fe doped MoS_2 (denoted as Cr–MoS_2 and Fe–MoS_2, respectively). The structure, spin charge density (SCD) derived from the difference in the charge density between the spin-up and spin-down channels, band structures, and density of states (DOS) of single Cr/Fe doped MoS_2 are shown in Fig. 1. As shown in Fig. 1(b), there is obvious asymmetry between the spin-up and spin-down channels for Cr doped MoS_2 around the Fermi level, which indicates that Cr doping can induce spin-polarized states. However, although the Cr atom shows a −2.689 μ_B local magnetic moment, the total magnetic moment of the system is 0 μ_B. The SCD as shown in Fig. 1(a) indicates that the antiferromagnetic Cr couples with its neighboring S/Mo atoms. Each of its six nearest neighbor (NN) S atoms shows a 0.117 μ_B magnetic moment, and each of its six neighboring Mo atoms shows a 0.229 μ_B magnetic moment. The Cr doped MoS_2 still behaves as a semiconductor, however, although the system shows zero total magnetic moment, its valence band maximum (VBM) is totally spin-polarized.

Open Access Article. Published on 06 April 2017. Downloaded on 1/20/2026 4:31:29 AM.
This article is licensed under a Creative Commons Attribution-NonCommercial 3.0 Unported Licence.

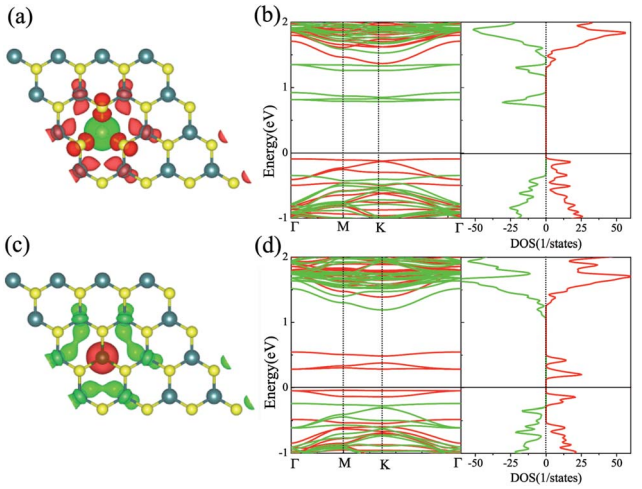

Fig. 1 The structure and SCD of the single Cr (a) and Fe (c) doped monolayer MoS_2. The isosurface of the SCD is 0.005 e $Å^{-3}$. (b) and (d) are the band structures and DOS for Cr–MoS_2 and Fe–MoS_2, respectively.

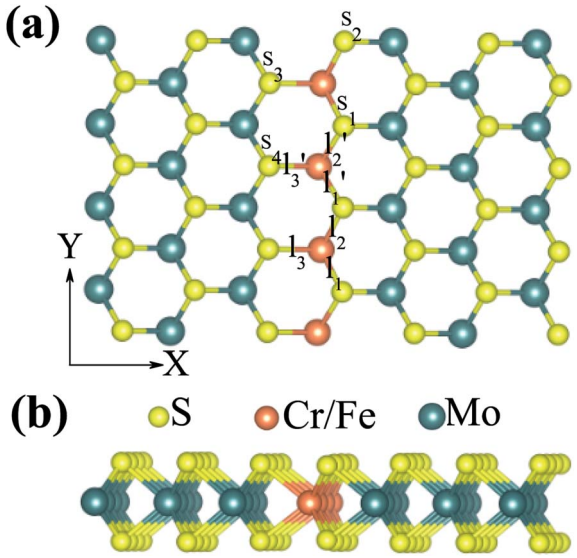

Fig. 2 (a) Top and (b) side view of the δ-type doped monolayer MoS_2.

Moreover, the impurity states in the band gap derived from the d state of Cr and the conduction band minimum (CBM) show opposite spin-polarization with that of the VBM, indicting that the system behaves as a bipolar magnetic semiconductor (BMS) as proposed by Li *et al.*[47] The difference between our work and the previous report[35] is derived from the different treatment of the on site Hubbard U correction. As for the Fe doped MoS_2, the ferromagnetic Fe couples with its NN S, whereas the antiferromagnetic Fe couples with its NN Mo, as shown in Fig. 1(c). The local magnetic moments of Fe and its neighboring S/Mo are 3.559 μ_B, 0.038 μ_B/−0.264 μ_B, respectively, and the total magnetic moment of the system is 2 μ_B. The band structure and DOS of the Fe doped system indicate that the system behaves as a spin-polarized semiconductor (SPS).

Then, we studied the modulation effect of Cr and Fe δ-type doping and Cr/Fe δ codoping on the electronic and magnetic properties of the monolayer MoS_2. The δ-type doping is along the zigzag direction of the monolayer MoS_2 and the Mo atoms are substituted with Cr, Fe, or alternatively Fe and Cr, with the model being shown in Fig. 2. We named the Cr and Fe δ-type doping systems as CrCr-chain-MoS_2 and FeFe-chain-MoS_2, respectively. For the Cr and Fe δ-type alternatively codoped systems, we considered two configurations, named FeFeCrCr-chain-MoS_2 and FeCrFeCr-chain-MoS_2. To estimate the stability of the four δ-type doping configurations, the average binding energy (E_b) was calculated as

$$E_b = (E_v + xE_{Cr} + yE_{Fe} - E_{TM\text{-}MoS_2})/m \quad (1)$$

where the term E_v is the energy of a relaxed MoS_2 monolayer with m Mo vacancies, and E_{Fe} and E_{Cr} are the energy of x and y isolated Fe and Cr atoms, respectively. $E_{TM\text{-}MoS_2}$ is the energy of a relaxed MoS_2 monolayer with Cr/Fe δ-type doping. $m = x + y$ is the number of TM atoms in the corresponding δ-type doped configuration. The value of m is 2, 2, 2, and 4 for the CrCr-chain-MoS_2, FeFe-chain-MoS_2, FeCrFeCr-chain-MoS_2, and FeFeCrCr-chain-MoS_2 configurations, respectively. The calculated E_b values are shown in Table 1. The results indicate that all of the binding energies are positive and larger than 5 eV, which demonstrates that the MoS_2 monolayer with δ-type doping of Cr and Fe is more stable than the single Fe and Cr doped MoS_2 monolayers as reported previously.[35]

Previous studies have shown that monolayer MoS_2 appears to be magnetic after being doped with TM atoms,[29,30] thus we should firstly consider the magnetic exchange coupling between Cr and Fe, which determines the magnetic order of Cr/Fe-chain-MoS_2. To ascertain the stable magnetic state, we calculate the energy of the antiferromagnetic and ferromagnetic states for all systems, and define δE as the energy difference between the ferromagnetic and antiferromagnetic states, with the results being listed in Table 1. One can see that the systems which are antiferromagnetic are more favorable in energy than the system in the ferromagnetic state, except for FeFe-chain-MoS_2. As listed in Table 1, the results show that CrCr-chain-MoS_2, FeFeCrCr-chain-MoS_2, and CrFeCrFe-chain-MoS_2 in the antiferromagnetic state are 444 meV, 509 meV and 325 meV energetically lower than the system in the ferromagnetic state, respectively. The large difference is favorable for their high temperature application. However, for FeFe-chain-MoS_2, which shows ferromagnetic coupling, its energy under the ferromagnetic state is 150 meV lower than that of the antiferromagnetic one. The results indicate that the four configurations have robust antiferromagnetic and ferromagnetic orders. To explore the electronic properties of the δ-type doped systems, we calculated their total density of states (TDOS) corresponding to stable magnetic ordering and the results are shown in Fig. 3. The results indicate that CrCr-chain-MoS_2 is an anti-ferromagnetic semiconductor with a narrower band gap of about 0.6 eV, FeFeCrCr-chain-MoS_2 is an anti-ferromagnetic spin-polarized metal and its spin-polarization at the Fermi level is up to

This journal is © The Royal Society of Chemistry 2017

Open Access Article. Published on 06 April 2017. Downloaded on 1/20/2026 4:31:29 AM.
This article is licensed under a Creative Commons Attribution-NonCommercial 3.0 Unported Licence.

Table 1 The calculated results of the Cr and Fe δ-type doped MoS_2. E_b denotes the average binding energy of the systems. The term 'M' is the total magnetic moment of the unit cell. The magnetic moments of the doped Cr (M_{Cr2}) and Fe (M_{Fe1}) in the unit cell are also shown. δE is the energy difference defined as $\delta E = E_{FM} - E_{AFM}$, where E_{FM} and E_{AFM} are the total energies for the ferromagnetic and antiferromagnetic states in the same unit cell, respectively

	E_b (eV)	Magnetic states	M (μ_B)	M_{Cr1} (μ_B)	M_{Cr2} (μ_B)	M_{Fe1} (μ_B)	M_{Fe2} (μ_B)	δE (meV)
CrCr-chain-MoS_2	5.078	AFM	0	−2.908	2.908	—	—	444
FeFe-chain-MoS_2	5.126	FM	8	—	—	3.156	3.159	−150
FeFeCrCr-chain-MoS_2	5.010	AFM	0	3.084	−3.005	−3.347	3.661	509
FeCrFeCr-chain-MoS_2	5.224	AFM	2	−3.019	—	3.499	—	325

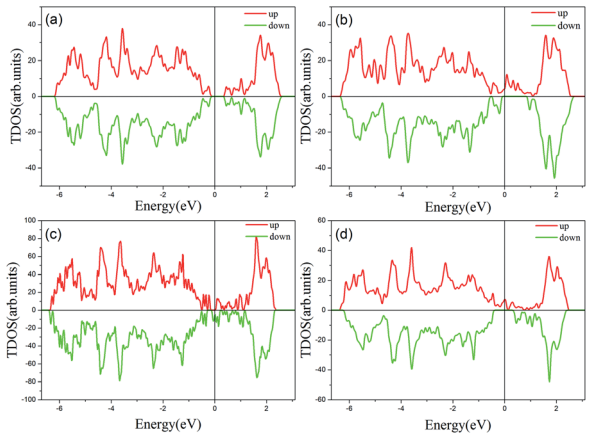

Fig. 3 The total density of states (TDOS) of Cr and Fe δ-type doping in monolayer MoS_2. The results of FeFe-chain-MoS_2, CrCr-chain-MoS_2, FeFeCrCr-chain-MoS_2, and FeCrFeCr-chain-MoS_2 are shown in (a), (b), (c), and (d), respectively. The Fermi level is set to zero.

92.5%, FeFe-chain-MoS_2 behaves as a half-metal with 100% spin polarization at the Fermi level, and FeCrFeCr-chain-MoS_2 is a HMFi' with 100% spin-polarization at the Fermi level although the neighboring Fe and Cr show anti-ferromagnetic coupling. To clearly understand the magnetic order, the spin-polarized charge densities (SCDs) were calculated and the results are presented in Fig. 4. The results indicate that the majority and minority SCDs are mainly concentrated around the Cr/Fe chain, and Cr/Fe induces a small spin polarization on its NN S/Mo. As for FeFe-chain-MoS_2, Fe and its NN Fe share the same spin-polarization and magnetic moment, while the spin-polarization and magnetic moments of Cr with its NN Cr in CrCr-chain-MoS_2 are opposite. Moreover, from Fig. 4(b), one can find that the Fe atoms of FeFe-chain-MoS_2 are antiferromagnetically coupled with its NN S/Mo atoms. For the FeFeCrCr-chain-MoS_2 system, as shown in Fig. 4(c), the magnetic couplings between Fe and its NN Fe as well as its NN Cr are antiferromagnetic, and the local magnetic moments of Fe1 and Fe2 (Cr1 and Cr2) in the unit cell have nearly the same values as the opposite direction, thus the overall magnetic moment of the system is zero. Although Cr and its NN Fe in FrCrFeCr-chain-MoS_2 are antiferromagnetically coupled as shown in Fig. 4(d), the total magnetic moment of this system is 2 μ_B so it is behaving as a ferrimagnet, and the origin of this magnetism will be discussed below. The above results indicate that Cr and Fe δ doping are effective approaches to modulate the electronic and magnetic properties of MoS_2. In particular, FeCrFeCr-chain-MoS_2 behaves as a HMFi' with 100% spin-polarization at the Fermi level, whose detailed magnetic coupling mechanism will be emphasized below.

As discussed above, FeCrFeCr-chain-MoS_2 behaves as a ferrimagnetic half-metal. We will focus on the origin of HMFi' and its electronic structures. Its band structures are shown in Fig. 5, where one can see that the system is a half-metal; the

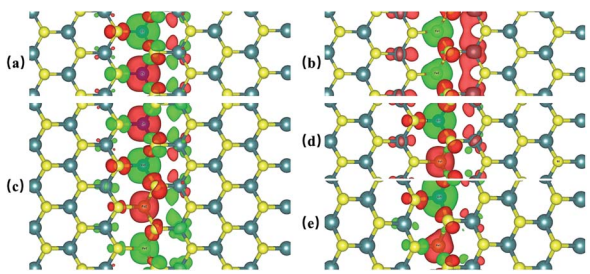

Fig. 4 The spin charge density (SCD) of CrCr-chain-MoS_2 (a), FeFe-chain-MoS_2 (b), FeFeCrCr-chain-MoS_2 (c), and FeCrFeCr-chain-MoS_2 (d). (e) is the SCD of FeCrFeCr-chain-MoS_2 under 12% compressed strain. The isosurface of the SCD is 0.005 e $Å^{-3}$. The red and blue isosurfaces denote the majority and minority spin channels, respectively.

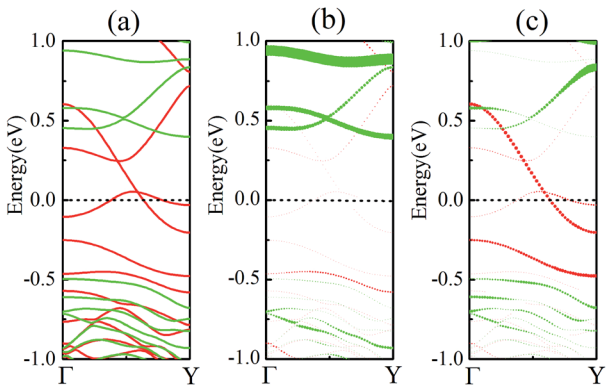

Fig. 5 (a) Band structures of FeCrFeCr-chain-MoS_2, with the red and green lines representing the majority and minority spin channels, respectively. The projector of the bands of Cr and Fe are described in (b) and (c), respectively. The Fermi level is set to zero.

Open Access Article. Published on 06 April 2017. Downloaded on 1/20/2026 4:31:29 AM.
This article is licensed under a Creative Commons Attribution-NonCommercial 3.0 Unported Licence.

spin-up channel is metallic while the spin-down channel is semiconducting with a gap (E_g) of 0.9 eV approximately. From the projection of the bands as shown in Fig. 5(b) and (c), we can see that the electrons at the Fermi level of the system are mainly derived from Fe. As mentioned above, the SCD in Fig. 4(d) indicates that Cr and Fe are anti-ferromagnetically coupled and most majority and minority SCDs localize around Fe and Cr, respectively. The band structures as shown in Fig. 5(b) and (c) indicate that around the Fermi level only the 3d states of Fe exist, and both the occupied and unoccupied 3d states of Cr are away from the Fermi level, resulting in the half-metallic characteristics of FeCrFeCr-chain-MoS_2. As for the pristine monolayer MoS_2, each Mo atom has six equivalent Mo–S bonds. Symmetry analysis shows that the pristine MoS_2 system presents D_{3h} symmetry. The NN S atoms of Cr/Fe in the codoped system will be no longer equivalent. However, S_1 and S_2, as indicated in Fig. 1, show a slight difference so they can be treated as equivalent. The total magnetic moment of FeCrFeCr-chain-MoS_2 is 2 μ_B per unit cell, which follows the Slater–Pauling rule:[48] $M_t = Z_t - 24$, where Z_t is the total number of valence electrons. The magnetic moments of the Cr and Fe atoms are -3.019 μ_B and 3.499 μ_B, respectively. Moreover, the Cr and Fe atoms further induce relatively small magnetic moments on their surrounding S and Mo atoms due to the proximity effect. The magnetic coupling between Fe and its neighboring S is ferromagnetic, while the coupling between Cr and its neighboring S is antiferromagnetic. The magnetic moments of the S atoms depend on the distance between S and Fe/Cr. S_1 and S_2 (as denoted in Fig. 1) have the same spin magnetic moments, and the magnetic moment of S_3 is smaller than S_1 and S_2 but larger than S_4, because the distance between S and Fe/Cr shows the sequence of $\ell_1 = \ell_2 < \ell_3$, $\ell'_1 = \ell'_2 < \ell'_3$ (the ℓs were denoted in Fig. 1). The magnetic moments of S_1, S_2, S_3, and S_4 are 0.115 μ_B, 0.115 μ_B, 0.083 μ_B, and 0.033 μ_B, respectively, and the magnetic moments of the four next nearest neighbor (NNN) Mo atoms of Fe/Cr are 0.111 μ_B, 0.110 μ_B, 0.127 μ_B, 0.128 μ_B, respectively. In comparison with the free state, the magnetic moments of Cr and Fe are reduced due to the 4s electrons of Cr and Fe being transferred to MoS_2 and the redistribution of the 3d electrons of Cr and Fe. To evaluate the charge transfer between Cr/Fe and MoS_2, we calculated the atomic basin charge based on the atoms in molecules (AIM) theory.[49] The results indicate that about one electron from the Cr/Fe atom transfers to the nearest neighbor S atom. Such electron transfer also produces a slight increase in the number of electrons in their NNN Mo atoms.

To further comprehend the mechanism of half-metallicity in FeCrFeCr-chain-MoS_2, we show the partial density of states (PDOS) of Cr/Fe and their NN S atoms in Fig. 6. The 3d orbitals of Cr and Fe can be split into three classes: A1(d_{z^2}), E1(d_{yz}, d_{xz}), and E2(d_{xy}, $d_{x^2-y^2}$). As for the case of the Cr atom, in the spin-down channel, the results indicate that the A1 states are nearly occupied, and there are some unoccupied E1 and E2 state peaks located around 0.4 eV and 0.9 eV, respectively. According to the integration of the d state of the PDOS of Cr, the Cr atomic spin configuration is close to $d^{0\uparrow}d^{3\downarrow}$. Whereas, the d states of Fe below the Fermi level are predominantly in the majority

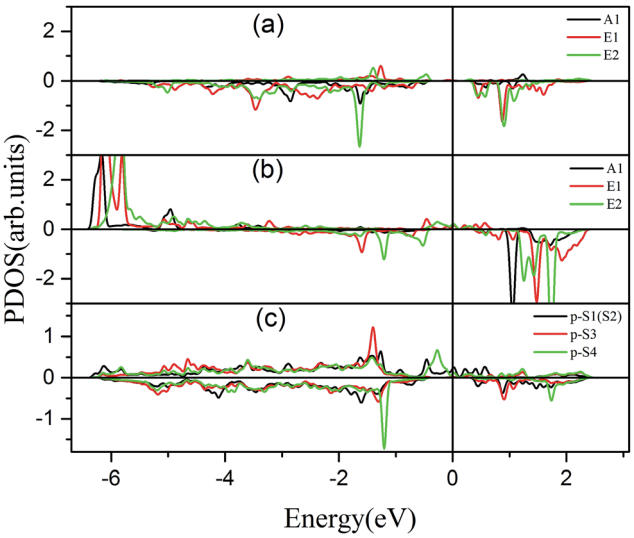

Fig. 6 Partial density of states (PDOS) of the d orbital of Cr (a) and Fe (b). (c) is the PDOS of the p orbitals of $S_{1(2)}$, S_3, and S_4. The positive and negative values denote the majority and minority channels, respectively. The Fermi level is set to zero.

channel, where the main peaks lie at around -6.0 eV. For the minority spin channel, the E1 and E2 states of Fe are partly occupied within a [-2.0 eV, -0.5 eV] energy window. Furthermore, the similar minority peaks for Cr and Fe around -1.7 eV indicate their coupling effect. It is worth mentioning that $S_{1(2)}$ has a peak in the same position, which proves that the interaction between Cr and Fe is mediated by the S between them. The Fe atomic spin configuration is close to $d^{5\uparrow}d^{1\downarrow}$ according to the integration of the d state of the PDOS of Fe. Contrary to Cr, with the results shown in Fig. 6(b), we can also notice that there are majority E1 and E2 states of Fe at the Fermi level. Meanwhile, the majority p states of $S_{1(2)}$ and S_3 locate around the Fermi level indicating the coupling between $S_{1(2)}$ and S_3 and Fe. Although there are Fe:3d–Cr:3d hybridizations through the mediating S, most of the Fe:3d majority remains non-bonding and is located around the Fermi level. Therefore, as far as the spin-up channel is concerned, FeCrFeCr-chain-MoS_2 behaves as a metal.

The PDOS of Cr and Fe indicate that the exchange splitting is opposite for the 3d states of Cr and Fe. Such behavior makes the local magnetic moments of the two transition-metal cations antiparallel. Therefore, we take a simplified model to analyze the magnetic coupling mechanism between Cr and Fe, as illustrated in Fig. 7. The virtual hopping of electrons between the p state of S_1 and d state of Cr (Fe) follows Goodenough–Kanamori–Anderson (GKA)[50,51] rules. In the model, the bond angle of Fe–S_1–Cr is 83.99° (close to 90°), hence we could analyse it with 90° configurations. The p_π orbital of S_1 is only non-orthogonal to d_{xy}, so consequently a partial covalent bond between the p_π and dε [d_{xy}] states will form. Then the electron virtual hopping occurs from the p_π orbital with the spin down state $|\downarrow>$ to the same unoccupied state of Fe due to Pauli's exclusion principle. The remaining p_σ orbital (spin-up state), which is non-orthogonal to dε', antiferromagnetically couples to

This journal is © The Royal Society of Chemistry 2017

Open Access Article. Published on 06 April 2017. Downloaded on 1/20/2026 4:31:29 AM.
This article is licensed under a Creative Commons Attribution-NonCommercial 3.0 Unported Licence.

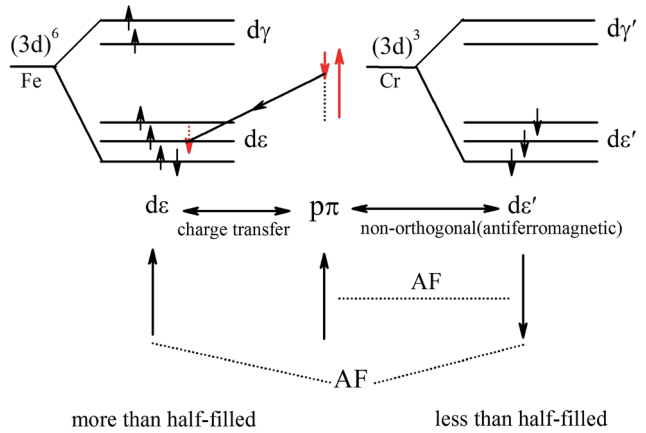

Fig. 7 Schematic of the virtual hopping between the d orbitals of Fe and Cr under AFM coupling.

the dε′ orbitals of Cr. Thus the resultant superexchange interaction between Cr and Fe is antiferromagnetically coupled.

As mentioned above, FeCrFeCr-chain-MoS_2 behaves as a HMFi', showing a net 2 μ_B magnetic moment per unit-cell. Such magnetic properties will form a stray field in the system, which inevitably reduces the efficiency of the spin filter along the δ-type TM nano wire. Theoretical calculations have proven that external strain is an effective method to modulate the magnetism of 2D systems.[32,52,53] We find that when we applied 12% compressed strain along the direction of the *x*-axis, the total magnetic moment can be reduced from 2 μ_B to 0 μ_B. Moreover, under such strain, antiferromagnetic coupling is still the favorable state for the system as the SCD results indicated in Fig. 4(e). The band structures of FeCrFeCr-chain-MoS_2 under 12% compression, as shown in Fig. 8(a), indicate that the system transforms to a half-semiconductor, in which the VBM and CBM are fully spin-polarized with the same spin-up channel exhibiting about a 0.3 eV band gap. Fig. 8(b) and (c) show that the states of the VBM result from Fe and the states of the CBM derive from the hybrid of Cr and Fe. The results indicate that the

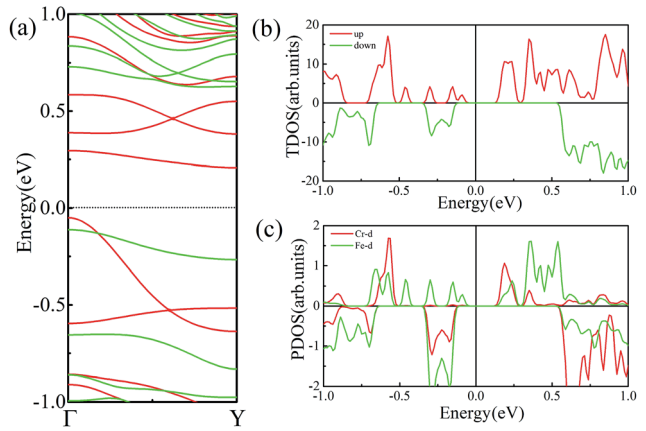

Fig. 8 (a) Band structures of FeCrFeCr-chain-MoS_2 under 12% compression strain. The Fermi level is set to zero. The TDOS and PDOS of Cr and Fe d orbitals are shown in (b) and (c), respectively.

magnetic properties of FeCrFeCr-chain-MoS_2 can be effectively modulated with external strain producing its flexibility for applications in spintronics. Finally, it is worth noting that there are a lot of reports[54,55] on the line defects in two dimensional MoS_2 in experiments which may be the templates of the δ type doping. Considering the interesting properties of Fe/Cr δ type doped MoS_2, we are looking forward to the confirmation in experiments soon.

4 Conclusions

In the present work, we employed first-principles calculations to study the electronic and magnetic properties of Cr and Fe δ-type doped single layer MoS_2. Our results demonstrate that Cr and Fe δ-type doping greatly influences the magnetic and electronic properties of monolayer MoS_2, especially in the Cr and Fe alternatively codoped monolayer MoS_2 (FeCrFeCr-chain-MoS_2) which exhibits half-metallic ferrimagnetic properties with a 2 μ_B magnetic moment per unit cell. We analyzed the magnetic interaction of Cr/Fe and the nearest neighbor S atom, and found an interesting phenomenon: S is ferromagnetically coupled with Fe, and simultaneously antiferromagnetically coupled with Cr. Subsequently, we applied strain to modulate the magnetism. The magnetic moment turns from an initial 2 μ_B to 0 μ_B under 12% compression along the *x*-axis. The half-metallic ferrimagnetism in the monolayer MoS_2 not only provides potential applications in spintronics, but also offers guidance for the implementation of half-metallic antiferromagnetism in two-dimensional materials.

Acknowledgements

This work is supported by the National Natural Science Foundation of China (Grant No. 11574260) and scientific research innovation project of Hunan Province (CX2015B219).

References

1 R. A. de Groot, F. M. Mueller, P. G. v. Engen and K. H. J. Buschow, *Phys. Rev. Lett.*, 1983, **50**, 2024–2027.
2 B. I. Min, M. S. Park and J. H. Park, *J. Phys.: Condens. Matter*, 2004, **16**, S5509.
3 X. Hu, *Adv. Mater.*, 2012, **24**, 294–298.
4 K. Schwarz, *J. Phys. F: Met. Phys.*, 1986, **16**, L211.
5 M. Shirai, T. Ogawa, I. Kitagawa and N. Suzuki, *J. Magn. Magn. Mater.*, 1998, **177**, 1383–1384.
6 H. van Leuken and R. A. de Groot, *Phys. Rev. Lett.*, 1995, **74**, 1171–1173.
7 W. E. Pickett, *Phys. Rev. Lett.*, 1996, **77**, 3185–3188.
8 W. E. Pickett, *Phys. Rev. B*, 1998, **57**, 10613–10619.
9 D. Ködderitzsch, W. Hergert, Z. Szotek and W. M. Temmerman, *Phys. Rev. B*, 2003, **68**, 125114.
10 M. Nakao, *Phys. Rev. B*, 2008, **77**, 134414.
11 H. Akai and M. Ogura, *Phys. Rev. Lett.*, 2006, **97**, 026401.
12 I. Galanakis, P. Dederichs and N. Papanikolaou, *Phys. Rev. B*, 2002, **66**, 174429.

Open Access Article. Published on 06 April 2017. Downloaded on 1/20/2026 4:31:29 AM. This article is licensed under a Creative Commons Attribution-NonCommercial 3.0 Unported Licence.

13 B. Huang, H. Xiang, J. Yu and S.-H. Wei, *Phys. Rev. Lett.*, 2012, **108**, 206802.
14 J. He, P. Zhou, N. Jiao, X. Chen, W. Lu and L. Z. Sun, *RSC Adv.*, 2015, **5**, 46640–46647.
15 J. He, P. Lyu, L. Z. Sun, A. Morales Garcia and P. Nachtigall, *J. Mater. Chem. C*, 2016, **4**, 6500–6509.
16 K. F. Mak, C. Lee, J. Hone, J. Shan and T. F. Heinz, *Phys. Rev. Lett.*, 2010, **105**, 136805.
17 B. Radisavljevic, A. Radenovic, J. Brivio, i. V. Giacometti and A. Kis, *Nat. Nanotechnol.*, 2011, **6**, 147–150.
18 Z. Yin, H. Li, H. Li, L. Jiang, Y. Shi, Y. Sun, G. Lu, Q. Zhang, X. Chen and H. Zhang, *ACS Nano*, 2012, **6**, 74–80.
19 F. K. Perkins, A. L. Friedman, E. Cobas, P. M. Campbell, G. G. Jernigan and B. T. Jonker, *Nano Lett.*, 2013, **13**, 668–673.
20 K. Chang and W. Chen, *ACS Nano*, 2011, **5**, 4720–4728.
21 N. Choudhary, J. Park, J. Y. Hwang and W. Choi, *ACS Appl. Mater. Interfaces*, 2014, **6**, 21215–21222.
22 X. Gu, W. Cui, H. Li, Z. Wu, Z. Zeng, S.-T. Lee, H. Zhang and B. Sun, *Adv. Energy Mater.*, 2013, **3**, 1262–1268.
23 Y.-H. Lee, X.-Q. Zhang, W. Zhang, M.-T. Chang, C.-T. Lin, K.-D. Chang, Y.-C. Yu, J. T.-W. Wang, C.-S. Chang, L.-J. Li, *et al.*, *Adv. Mater.*, 2012, **24**, 2320–2325.
24 J. N. Coleman, M. Lotya, A. ONeill, S. D. Bergin, P. J. King, U. Khan, K. Young, A. Gaucher, S. De, R. J. Smith, *et al.*, *Science*, 2011, **331**, 568–571.
25 B. Radisavljevic, A. Radenovic, J. Brivio, V. Giacometti and A. Kis, *Nat. Nanotechnol.*, 2011, **6**, 147–150.
26 M. Heyne, D. Chiappe, J. Meersschaut, T. Nuytten, T. Conard, H. Bender, C. Huyghebaert, I. P. Radu, M. Caymax, J.-F. de Marneffe, *et al.*, *J. Mater. Chem. C*, 2016, **4**, 1295–1304.
27 S. Ghosh, S. Najmaei, S. Kar, R. Vajtai, J. Lou, N. Pradhan, L. Balicas, P. Ajayan and S. Talapatra, *Phys. Rev. B*, 2014, **89**, 125422.
28 Y. Li, Z. Zhou, S. Zhang and Z. Chen, *J. Am. Chem. Soc.*, 2008, **130**, 16739–16744.
29 Y. Wang, B. Wang, R. Huang, B. Gao, F. Kong and Q. Zhang, *Phys. E*, 2014, **63**, 276–282.
30 X.-Q. Wang, W.-G. Chen, Z.-L. Zhu and Y. Jia, *Acta Metall. Sin. (Engl. Lett.)*, 2015, **28**, 793–798.
31 K. Dolui, I. Rungger, C. D. Pemmaraju and S. Sanvito, *Phys. Rev. B*, 2013, **88**, 075420.
32 J. Qi, X. Li, X. Chen and K. Hu, *J. Phys.: Condens. Matter*, 2014, **26**, 256003.
33 A. Ramasubramaniam and D. Naveh, *Phys. Rev. B*, 2013, **87**, 195201.
34 Y. Wang, S. Li and J. Yi, *Sci. Rep.*, 2016, **6**, 24153.
35 Q. Yue, S. Chang, S. Qin and J. Li, *Phys. Lett. A*, 2013, **377**, 1362–1367.
36 Y. Cheng, Z. Zhu, W. Mi, Z. Guo and U. Schwingenschlögl, *Phys. Rev. B*, 2013, **87**, 100401.
37 P. Hohenberg and W. Kohn, *Phys. Rev.*, 1964, **136**, B864–B871.
38 W. Kohn and L. J. Sham, *Phys. Rev.*, 1965, **140**, A1133.
39 G. Kresse and J. Furthmüller, *Phys. Rev. B*, 1996, **54**, 11169.
40 G. Kresse and J. Furthmüller, *Comput. Mater. Sci.*, 1996, **6**, 15–50.
41 W. Yao, E. Wang, H. Huang, K. Deng, M. Yan, K. Zhang, K. Miyamoto, T. Okuda, L. Li, Y. Wang, H. Gao, C. Liu, W. Duan and S. Zhou, *Nat. Commun.*, 2017, **8**, 14216.
42 M. Garnica, D. Stradi, S. Barja, F. Calleja, C. Diaz, M. Alcami, N. Martin, A. L. Vazquez de Parga, F. Martin and R. Miranda, *Nat. Phys.*, 2013, **9**, 368–374.
43 P. E. Blöchl, *Phys. Rev. B*, 1994, **50**, 17953.
44 G. Kresse and D. Joubert, *Phys. Rev. B*, 1999, **59**, 1758.
45 J. P. Perdew, K. Burke and M. Ernzerhof, *Phys. Rev. Lett.*, 1996, **77**, 3865.
46 V. I. Anisimov, F. Aryasetiawan and A. Lichtenstein, *J. Phys.: Condens. Matter*, 1997, **9**, 767.
47 X. Li, X. Wu, Z. Li, J. Yang and J. Hou, *Nanoscale*, 2012, **4**, 5680–5685.
48 I. Galanakis, K. Özdoğan, E. Şaşıoğlu and B. Aktaş, *Phys. Rev. B*, 2007, **75**, 092407.
49 R. Bader, *Atoms in Molecules: A Quantum Theory International Series of Monographs on Chemistry*, Clarendon Press, 1990.
50 J. B. Goodenough, *J. Phys. Chem. Solids*, 1958, **6**, 287–297.
51 J. B. Goodenough, *Phys. Rev.*, 1955, **100**, 564.
52 H. Shi, H. Pan, Y.-W. Zhang and B. I. Yakobson, *Phys. Rev. B*, 2013, **88**, 205305.
53 L. Kou, C. Tang, Y. Zhang, T. Heine, C. Chen and T. Frauenheim, *J. Phys. Chem. Lett.*, 2012, **3**, 2934–2941.
54 H.-P. Komsa, S. Kurasch, O. Lehtinen, U. Kaiser and A. V. Krasheninnikov, *Phys. Rev. B*, 2013, **88**, 035301.
55 Z. Zhang, X. Zou, V. H. Crespi and B. I. Yakobson, *ACS Nano*, 2013, **7**, 10475–10481.

 This journal is © The Royal Society of Chemistry 2017